Hindawi
Advances in Civil Engineering
Volume 2018, Article ID 1569683, 14 pages
https://doi.org/10.1155/2018/1569683

Research Article

Base Isolation of Buildings with Curved Surface Sliders: Basic Design Criteria and Critical Issues

Fernando Saitta,[1] Paolo Clemente,[1] Giacomo Buffarini,[1] Giovanni Bongiovanni,[1] Antonello Salvatori,[2] and Cristian Grossi[1]

[1]*ENEA Casaccia Research Centre, via Anguillarese 301, 00123 Rome, Italy*
[2]*University of L'Aquila, Via Giovanni Gronchi 18, 67100 L'Aquila, Italy*

Correspondence should be addressed to Paolo Clemente; paolo.clemente@enea.it

Received 27 March 2018; Revised 27 July 2018; Accepted 5 August 2018; Published 12 September 2018

Academic Editor: Evangelos J. Sapountzakis

Curved surface sliders are being used more and more in the seismic isolation of buildings. They are preferred not only because of their lower cost with respect to elastomeric isolators but also of their technical characteristics, such as the fact that the value of the period of vibration is independent of the mass and the automatic coincidence between the gravity mass center of the superstructure and the stiffness center of the isolation system. In this paper, these features are analysed with reference to simple structures, pointing out the possibility of rotations of the superstructure and the loss of contact in some devices. Finally, the importance of the static friction is also emphasized showing the experimental seismic response of an isolation system under a low-energy earthquake. For all these reasons, the use of nonlinear analysis, revised and detailed in this paper, is advisable for the isolation system made of curved surface sliders.

1. Introduction

In 1868, Stevenson developed an isolation system to protect the lighting system in Japan (Figure 1). It was called the "aseismatic joint" and consisted in spherical rollers in niches. These were likely the first isolation devices of modern conception and were similar to the modern curved surface sliders. Stevenson understood the basic concepts of seismic isolation very well: "It is evident that any sudden lateral motion of the earth, on which the building rests, must be communicated to the foundation of the structure, and thence through all the rigid and unyielding materials of which it is composed to its very summit, where the violence of the shock will be aggravated by the greater elevation of the highest point of the building above the source of motion. On fully considering this action of earthquakes, it occurred to me that what was required to neutralize their shocks was a *break* in the continuity of the rigid parts forming the structure, so as to prevent the propagation of the shock, with increasing violence from its foundation, to its summit. The idea being that, in some horizontal plane, the building should be cut through and separated, so that the sudden motion of the lower portion should not be directly communicated to the superincumbent building" [1].

A few years later, in 1970, Touaillon proposed a very similar isolation system that used spherical rollers in niches between superstructure and foundations; the return to the initial position was guaranteed by the elliptical geometry of the housing system.

These devices contained the basic concepts of the friction pendulum system (FPS), which was first developed in the USA in the early 90s of the last century. It made use of sliding elements covered with a special fabric. Later, the seismic isolation pendulum (SIP) was developed in Germany with polyethylene sliding materials and used in some applications also in Greece, Turkey, etc., and then with similar and other sliding materials, also in Italy. Nowadays, curved surface sliders (CSS) are widely used for buildings and bridges (Figure 2).

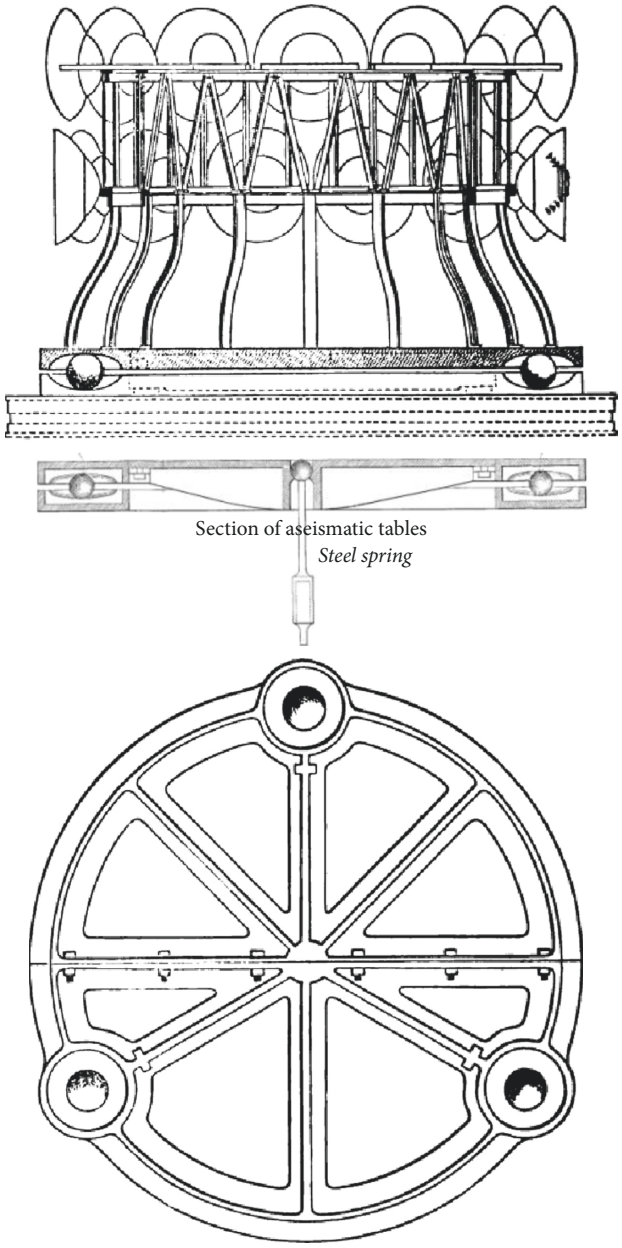

Figure 1: The aseismatic joint of Stevenson [1].

The success of the CSSs is essentially related to two reasons:

(i) The possibility of designing the isolation system independently of the effective mass of the superstructure

(ii) The automatic coincidence between the projection of center of the masses and the stiffness center, at least from a theoretical point of view

Furthermore, the cost of a CSS is usually lower than the cost of a high damped rubber bearing (HDRB).

In this paper, after a short introduction on seismic isolation and on the main features of the curved surface sliders, the behavior of buildings seismically isolated by means of single CSSs is analysed. The attention is focused on

Figure 2: Single curved surface slider.

the mathematical modelling of friction devices. Indeed, the original formulation [2] accounts for the variability of the friction coefficient with the sliding velocity, whereas other relevant aspects [3], such as the dependence on the contact pressure and the number of cycles, are usually neglected. In this paper, the effect of different friction coefficients for different isolators in the same building is examined, which corresponds to eccentricity of the stiffness center of the isolation layer with respect to the center of masses. The results of a numerical investigation are shown. This was carried out with reference to two simple framed structures, in which different distributions of the characteristics of the devices were considered. The analysis was performed using the acceleration time history recorded at L'Aquila during the 2009 earthquake. The study pointed out also the possibility of rotations of the superstructure and the loss of contact in some devices.

Finally, the importance of the static friction is emphasized showing the experimental seismic response of an isolation system under a low-energy earthquake. For all these reasons, the use of nonlinear analysis, revised and discussed in this paper, is advisable for the isolation system made of curved surface sliders.

2. Seismic Isolation and Curved Surface Sliders

It is well known that seismic isolation is based on the increasing of the fundamental period of vibration of the building, which corresponds to a terrific reduction of the seismic actions that affect the structure. Thanks to the filtering due to the seismic isolation system the superstructure is loaded by low seismic action and can support it in the elastic range, preserving the structure and its content [4].

The number of applications of seismic isolation increased rapidly all over the world [5]. As a matter of fact, several thousands of structures in the world are protected by new antiseismic techniques, located in more than thirty countries. The use of this new antiseismic system includes not only strategic structures (civil protection centers, army and police stations, etc.) and structures of relevant importance (schools, hospitals, hotels, theaters, airports, etc.) but also residential buildings and even small private houses. It also regards structures of all the types of material: reinforced concrete, steel, masonry, and even timber both for new constructions and the retrofit of existing buildings [6].

All the structures protected by seismic isolation exhibited an excellent behavior even under severe earthquakes. Most of the buildings showed no damage or very low damage, demonstrating that base isolation is a reliable technology for seismic protection of structures, ready for a wide application also in masonry and cultural heritage buildings [7, 8]. Furthermore, seismic monitoring systems are quite common also in base isolated buildings, providing several information on the actual seismic behavior of the base-isolated building under earthquakes of different energy [9, 10].

It must be noted that in some countries seismic isolation is considered as an additional safety measure, so the use of seismic isolation represents an additional construction cost. In other countries, among these is Italy, the seismic codes allow for the lowering of the seismic actions to the superstructure when using base isolation [11, 12]. In any case, it is important noting that when entrusting the safety of a building to a limited number of isolators, the reliability of these devices is a fundamental issue.

The isolation devices have first of all a bearing function. As a matter of fact, they have to support vertical loads always during their life, both in service conditions and under seismic actions. They should have a low horizontal stiffness, in order to allow relative displacements under seismic actions but also a suitable stiffness to avoid displacements in presence of low horizontal actions, such as wind and traffic-induced vibrations, and to guarantee a lateral constraint for them. Furthermore, they should have a good dissipation capacity, to lower the displacements under seismic actions, and a recentering capacity, to bring back the structure to its natural configuration after the event.

Curved surface sliders (CSS, Figure 3) are sliding isolators with curved surfaces that have, without the contribution of other elements, the following characteristics:

(i) The recentering capability, obviously due to curved surface, which allows the device to return to its initial position when the external horizontal action finishes

(ii) The energy dissipation, due to the friction between contact surfaces [13]

The behavior of a curved surface slider is similar to the behavior of a pendulum. An element sliding on a surface with a curvature radius R oscillates, for small amplitudes, with the period $T = 2\pi\sqrt{R/g}$, which is independent of the mass. This model represents well the behavior of a sliding pendulum only during the motion. It cannot account for what happens at the onset on motion and at the change of the velocity sign. In both cases, the behavior is governed by a static friction, which is usually much higher than the dynamic friction.

As shown in Figure 4, the motion of a curved surface slider is characterized by at least three phases, which corresponds to different friction factors: μ_0 is the static friction relative to the onset of motion; $\mu_{dyn} = \mu$ is the dynamic friction during the sliding with velocity similar to the design one; μ_1 is the friction factor corresponding to the change of velocity sign. It is $\mu < \mu_1 < \mu_0$. For velocity lower than

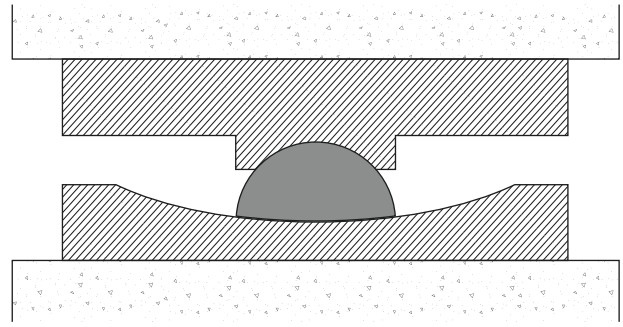

Figure 3: Schematic view of a single curved surface slider (CSS).

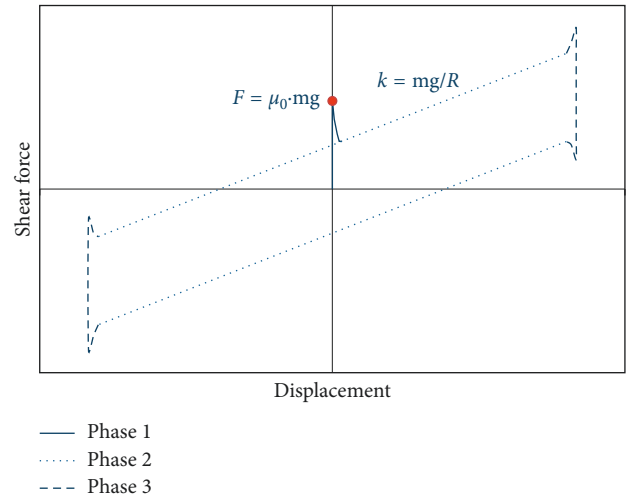

Figure 4: Effective force-displacement diagram of a CSS. The three different phases with different friction factors are apparent.

50 mm/s, a further static friction μ_{st} should be defined; it is used in the laboratory experimental analyses.

The model usually adopted for CSSs refers to a bilinear behavior. It is composed by an initial rigid phase and a linear phase, whose slope is given by $k = mg/R$ (Figure 5). With reference to the generic displacement d, the secant equivalent stiffness to be considered in the linear modelling, the period of vibration, and the damping are, respectively,

$$k_e = mg\left(\frac{1}{R} + \frac{\mu}{d}\right), \tag{1}$$

$$T_{is} = 2\pi\sqrt{\frac{1}{g(1/R + \mu/d)}}, \tag{2}$$

$$\xi_{is} = \frac{2}{\pi(d/R + \mu)}. \tag{3}$$

A fundamental parameter in the behavior of a CSS is its dynamic friction coefficient μ. The experimental analyses demonstrated that μ [14]

(i) decreases when the contact stress increases

(ii) gets up when the velocity increases from 0 to 150 mm/s and keeps constant for velocities between

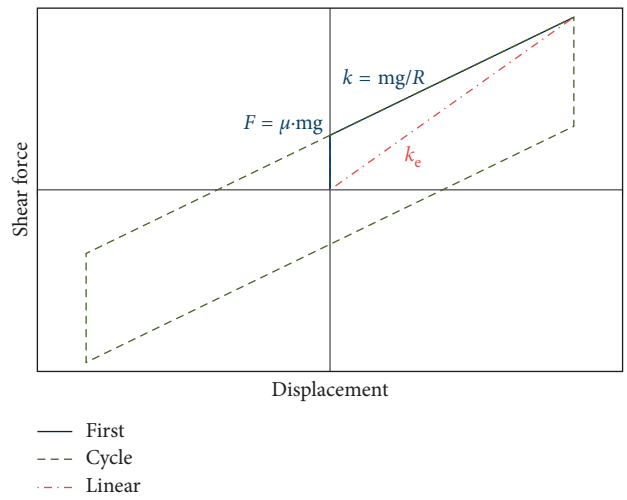

Figure 5: Ideal bilinear force-displacement diagram of a CSS.

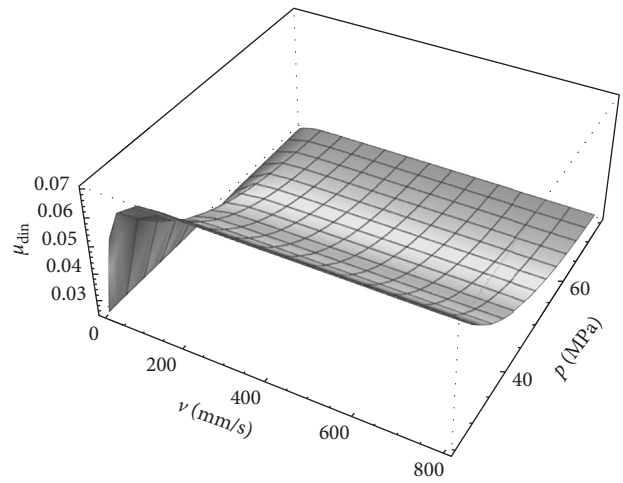

Figure 6: Typical diagram of the dynamic friction coefficient versus velocity and pressure.

200 and 800 mm/s, which are reached during the quake

(iii) decreases when the temperature increases

In Figure 6, the sliding coefficient of friction is plotted versus velocity v and pressure p.

With reference to the recentering, the shape and the friction play different roles. At positions corresponding to very low displacements, the recentering force is lower than the friction force. As a result, if the slider reaches the configuration with $d \le \mu R$ with velocity equal to zero, the device will not return to its initial configuration ($d = 0$). The value $d_{max} = \mu R$ is the maximum residual displacement.

Usually, the linear modelling is suitable only if some conditions are satisfied. These relate to

(i) the variability of the stiffness

(ii) the influence of the velocity and vertical load on friction

(iii) the increment of the force for high values of the displacement

The first and the third conditions imply two upper limits to the curvature radius. These are, respectively,

$$R < d \cdot \frac{\mu}{3}, \qquad R < 20 \cdot d. \tag{4}$$

3. Nonlinear Modelling of a CSS

The nonlinear modelling of the CSS behavior should account for

(i) the variability of the friction coefficient due to the variations of the vertical load and the sliding velocity

(ii) the rapid variations at the onset of motion and when the velocity sign changes

The influence of the sliding velocity v is described by the equation [15]:

$$\mu = f_{max} - (f_{max} - f_{min})e^{-\alpha|v|}, \tag{5}$$

where f_{max} is the friction coefficient at the high velocity, f_{min} is the friction coefficient at the very low velocity, and $1/\alpha$ is the characteristic sliding velocity. All these parameters are functions of the temperature. The parameter f_{max} is also influenced very much by the contact pressure p, while the influence of the contact pressure on f_{min} and α is lower and can be neglected. If $f_{max\,0}$ is the value for very low pressure and $f_{max\,p}$ the value for high pressure, the following expression is used:

$$f_{max} = f_{max\,0} - \left(f_{max\,0} - f_{max\,p}\right)\tanh(\varepsilon p), \tag{6}$$

where ε is a constant. The friction force is

$$F_f = \mu W \cdot Z. \tag{7}$$

Z is a nondimensional hysteresis variable that satisfies the equation [16, 17]:

$$\dot{Z} = \left(\frac{k}{\mu W}\right) \cdot v\left(1 - Z^2\right) \quad \text{if } v \cdot Z > 0, \qquad \dot{Z} = \left(\frac{k}{\mu W}\right) \cdot v \quad \text{if } v \cdot Z \le 0, \tag{8}$$

in which k represents the shear elastic stiffness of the sliding material in the absence of motion. During the motion, it is $Z = \pm 1$, while $|Z| < 1$ during the elastic behavior (Figure 7). This model interprets well the actual behavior, in which displacements of about 0.13/0.5 mm were observed experimentally between steel and PTFE (Teflon) during the rigid phase [2].

From the 1D model, the 2D model can be easily deduced. The forces-displacement relations are

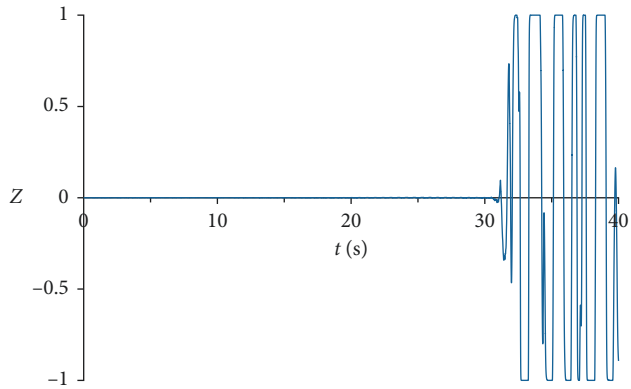

Figure 7: Z function in the case of seismic acceleration recorded during the 2009 L'Aquila earthquake.

$$F_x = \left(\frac{W}{R}\right) \cdot d_x + \mu_x W \cdot Z_x,$$
$$F_y = \left(\frac{W}{R}\right) \cdot d_y + \mu_y W \cdot Z_y, \tag{9}$$

and the friction coefficients depend on the resultant sliding velocity $v = (v_x^2 + v_y^2)^{1/2}$:

$$\mu_x = f_{\max,x} - \left(f_{\max,x} - f_{\min,x}\right)e^{-\alpha v},$$
$$\mu_y = f_{\max,y} - \left(f_{\max,y} - f_{\min,y}\right)e^{-\alpha v}. \tag{10}$$

The hysteresis variables are given by the differential equation system:

$$\begin{Bmatrix} \dot{Z}_x \\ \dot{Z}_y \end{Bmatrix} = \begin{bmatrix} 1 - \alpha_2 Z_x^2 & -\alpha_3 Z_x Z_y \\ -\alpha_2 Z_x Z_y & 1 - \alpha_3 Z_y^2 \end{bmatrix} \begin{Bmatrix} k_x/\mu_x W \cdot v_x \\ k_y/\mu_y W \cdot v_y \end{Bmatrix}, \tag{11}$$

where k_x and k_y are the elastic shear stiffness in the absence of sliding and α_2 and α_3 are equal to unity if $v_x Z_x > 0$ and $v_y Z_y > 0$, respectively, and equal to 0 elsewhere. The variables of hysteresis depend on the displacement, velocity, and initial stiffness k_i fixed by the yielding displacement. The interaction between the force components is governed by the condition $|Z| \le 1$. The system is at the yield point when $|Z| = 1$, otherwise it is in the elastic range. *SAP2000* software was used for the numerical analyses. The finite element friction-pendulum isolator was used, which accounts for the variation of the friction coefficient with the velocity but not of the contact pressure [18].

4. Vertical Displacement and Uplift

In the absence of uplift, a vertical component of the displacement is associated with a horizontal component. If ϑ is the arc length along the device, the horizontal and vertical components are, respectively,

$$d = R \sin \vartheta,$$
$$\delta_v = R(1 - \cos \vartheta). \tag{12}$$

In Figure 8, the nondimensional vertical displacement δ_v/R is plotted versus the nondimensional horizontal displacement d/R.

The vertical load acting on each device is influenced by the vertical seismic acceleration but also by the overturning moment due to the horizontal seismic actions. With reference to the first aspect, consider a plane frame of width B and total weight W, composed of n spans of equal length, and seismically isolated by means of one curved surface slider under each column (Figure 9). If S_e is the horizontal design acceleration, and the horizontal resultant force $F = S_e \cdot W$ is applied at the height H_g from the isolation plane, the effect on the first isolator is

$$\Delta W_1 = \frac{S_e W \cdot H_g}{B} + \sum \Delta W_i f_i(n, B). \tag{13}$$

where ΔW_i is the load variations on the other isolators due to the seismic action. By substituting $\Delta W_1 = 0.1 \cdot W_1$, we obtain the limit values for which the linear modelling is usually allowed according to the technical codes. If we suppose, for simplicity, $W_1 = W/2n$ the previous condition occurs when

$$\frac{H_g}{B} = \frac{(W/20n - \sum \Delta W_i f_i(n, B))}{S_e W}. \tag{14}$$

The curves relative to this case are plotted in Figure 10, for different values of n. The function $f_i(n, B)$ depends on the number of spans n and the width B. For $n = 3$, the previous relation becomes $H_g/B = (W/60 + \Delta W_1/3)/S_e W$.

5. Preliminary Design

The preliminary design of curved sliding devices is usually performed assuming constant values for the radius R, the vertical load W, and the friction μ. An iteration procedure can be used. This can be started by giving a first value d_1 for the displacement and calculating the stiffness K_{e1}, the period T_{is1}, and the damping ξ_{is1} from Equation (1). On the spectrum relative to ξ_{is1}, a new value d_2 of the displacement, corresponding to T_{is1}, can be obtained. If $d_2 \neq d_1$, the procedure is continued. It will be stopped when $d_i \approx d_{i-1}$ with a fixed tolerance.

6. Isolation Systems with CSS Devices Having Different Frictions

It has already been said that one of the most interesting characteristics of the CSSs is the automatic coincidence between the projection of center of the masses of the superstructure and the stiffness center of the isolators. This is not exactly true. Actually, the friction force at each device depends on the vertical load acting on it. First of all, the static vertical loads are not the same on all the devices. Furthermore, they vary during the earthquake, being related to the seismic overturning moment. The friction coefficient is also influenced by other phenomena. Among these, one of the most important phenomena is the cycling effect, which consists in the reduction of the friction coefficient with temperature. Therefore, some models have been proposed to

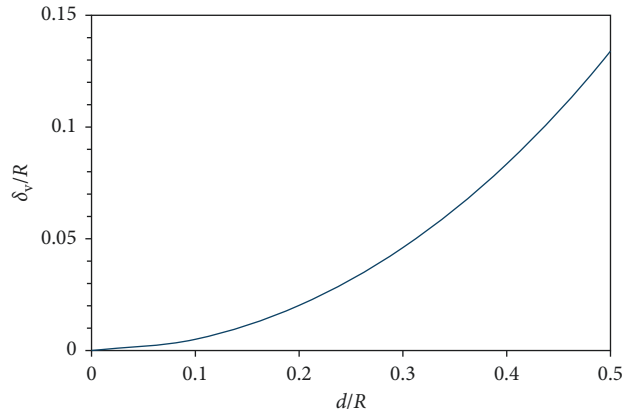

Figure 8: δ_v/R ratio versus d/R ratio.

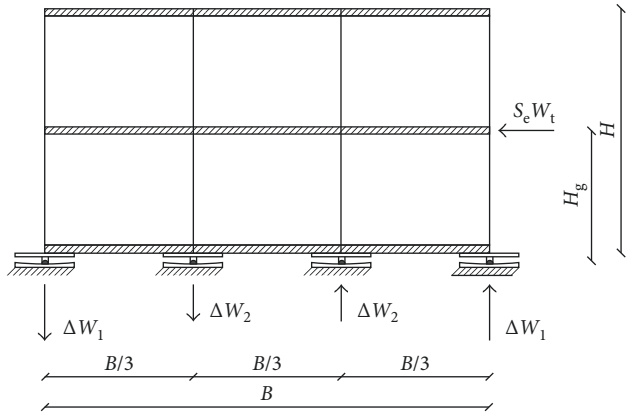

Figure 9: Plane frame with $n = 3$.

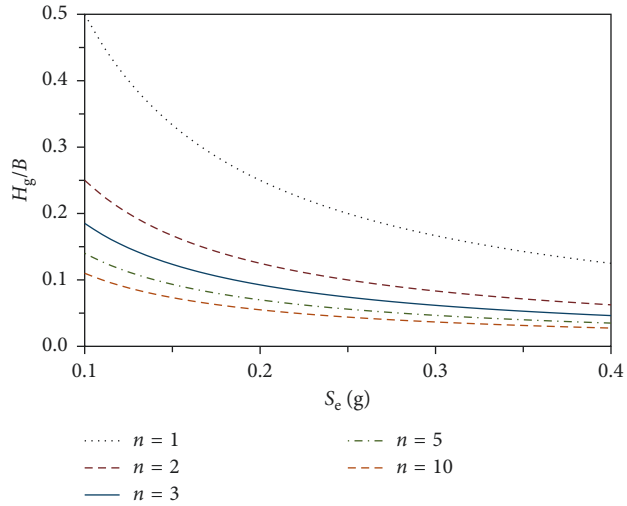

Figure 10: H_g/B ratio versus the design acceleration S_e for different values of n.

address all these aspects, usually not totally considered in commercial codes.

In the following, the responses of some simple spatial frames are analyzed, in which the friction coefficients of the isolators are not the same for all devices.

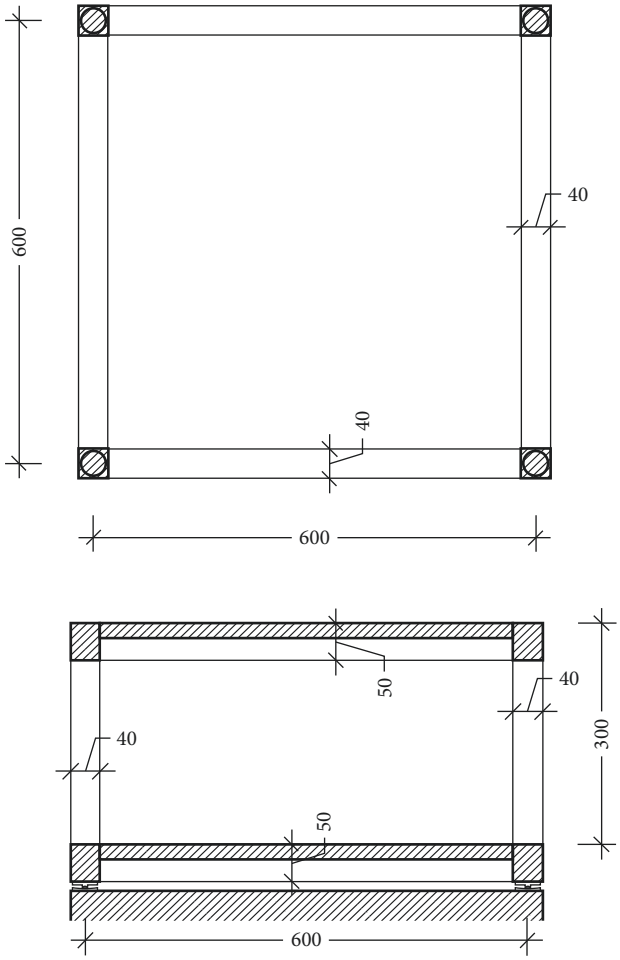

Figure 11: Four-column frame (dimensions in cm).

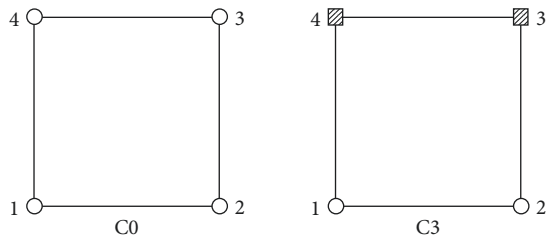

Figure 12: Four-column frame: different deployments of the sliding devices: circle = normal friction coefficient and square = increased friction coefficient.

Consider first the simple spatial frame in Figure 11. It is composed of two floors, with four columns at the corners, connected by beams at each floor. The columns have the same squared cross section. The beams have all the same rectangular cross sections. Therefore, the structure is symmetric around the two horizontal main axes. The structure is seismically isolated by means of four curved surface sliders placed under each column (C0 system, see Figure 12), characterized by a friction coefficient $\mu = 0.035$ for high speed and equal to 0.025 for low speed. The vertical load on each device is 1000 kN. A design displacement of 0.27 m was

Table 1: Characteristics of sliders.

Friction coefficient	μ	$1.5\,\mu$	$2.5\,\mu$
High-speed friction	0.035	0.0525	0.0875
Low-speed friction	0.025	0.0375	0.0625
Secant stiffness K_e(kN/m)	379.2	444.0	573.5
Elastic shear stiffness k (kN/m)	11438.2	13391.0	17296.8
Equivalent period T_{is} (s)	3.26	3.01	2.65

Table 2: Four-column frame: periods and participant masses (translation X, translation Y, and rotation Z in the vibration modes).

Mode no.	T(s)	Participant mass X	Participant mass Y	Participant mass RZ	Sum X	Sum Y	Sum RZ
1	3.259	0.001	0.999	0.335	0.001	0.999	0.335
2	3.259	0.999	0.001	0.389	1	1	0.724
3	2.104	0.000	0.000	0.276	1	1	1

considered. The previously described iteration procedure was used for the preliminary design of the sliding devices. The following design parameters were obtained and kept constant for all cases: radius $R = 4.0$ m, vertical stiffness $K_v = 2.1 \cdot 10^9$ kN/m, and $\alpha = 43$ s/m. The other characteristics are in the first column of Table 1 (μ).

The characteristics of the vibration modes, reported in Table 2, show that the first two modes of vibration have the same resonance frequency. They consist in translations only along the two main directions, respectively, and involve almost the total mass. In the third mode, the structure just rotates around its main vertical axis.

In order to introduce accidental asymmetry in the structure, the friction coefficients of one or two devices have been changed, assuming alternatively

(i) $\mu_a = 1.5\,\mu$, which corresponds to an equivalent viscous damping factor of 28%; the corresponding elastic and secant shear stiffness (in absence of sliding) were increased by about 20%,

(ii) $\mu_b = 2.5\,\mu$, which corresponds to an equivalent viscous damping factor of 36% and therefore is out of the technical range; it allowed to obtain a stiffness of the devices able to modify significantly the dynamic behavior of the system.

The characteristics of the isolation devices with these friction values are in the second and third columns of Table 1, respectively. Different cases were considered with reference to the isolator placements. The variation of the friction coefficient in one or more devices causes the reduction of the period of vibration but also the presence of important rotational component in the modal shapes. This is particularly evident in case C3 (Figure 12).

A nonlinear analysis (*fast nonlinear analysis*, FNA) was carried out by means of a finite element model with SAP2000, in which the inelastic effects were concentrated in a few points of the structural model. The structural damping was assumed to be equal to 5%. The three acceleration components recorded at the L'Aquila Park Station during the main shock of the 2009 earthquake were considered. The foundation of the models was first subjected to an acceleration component along the x axis. As one could expect, model C0 showed displacements along the x direction only, while model C3 presented also displacements along the y axis, which were higher in the case μ_b (Figure 13).

Then the model was subjected to the three acceleration components of the same seismic event, and the attention was focused on the vertical component of the displacement due to the curvature of the sliders. The software used does not account for this displacement component, which was evaluated separately. In the model with four columns, a maximum variation of the vertical load of about 60% was found. This allowed to state that no traction was present during the oscillation, and the vertical component of the displacement was well calculated. As shown in Figure 14, the vertical displacements were always the same in C0, while in model C3, it was verified that the maximum values were reached at the same time, and in any case, the contact points of the four sliders were on the same plane. The presence of traction in a device could determine the deformation of the superstructure needed to guarantee the contact; if the superstructure would not be able to absorb these deformations, the absence of contact would occur for a few instants.

Now consider the spatial frame in Figure 15, which differs from the previous one for the presence of a column just in the center of the frame (C10, see Figure 16). The vertical load was equal to 1800 kN on the central isolator device and equal to 535 kN on the others. Also in this case, a design displacement equal to 0.27 m was considered, and the values of $R = 4.0$ m, vertical stiffness $K_v = 2.1 \cdot 10^9$ kN/m, and $\alpha = 43$ s/m were assumed. The other characteristics of the sliding devices are in Tables 3 and 4, for the perimetral and the central isolators, respectively. As in the previous case, the first two modes of vibration have the same resonance frequency. These involve translations only in the two main directions, and the mass participation factor is very close to unity along the relative direction (Table 5).

In order to introduce accidental asymmetry in the structure, the characteristics of some devices were changed as in the previous case. The corresponding characteristics of the devices are in Tables 3 and 4 (columns 2 and 3). Also in this case, different distributions of the devices were considered. The models with friction coefficient increased in one or more device present modal shapes with lower period of

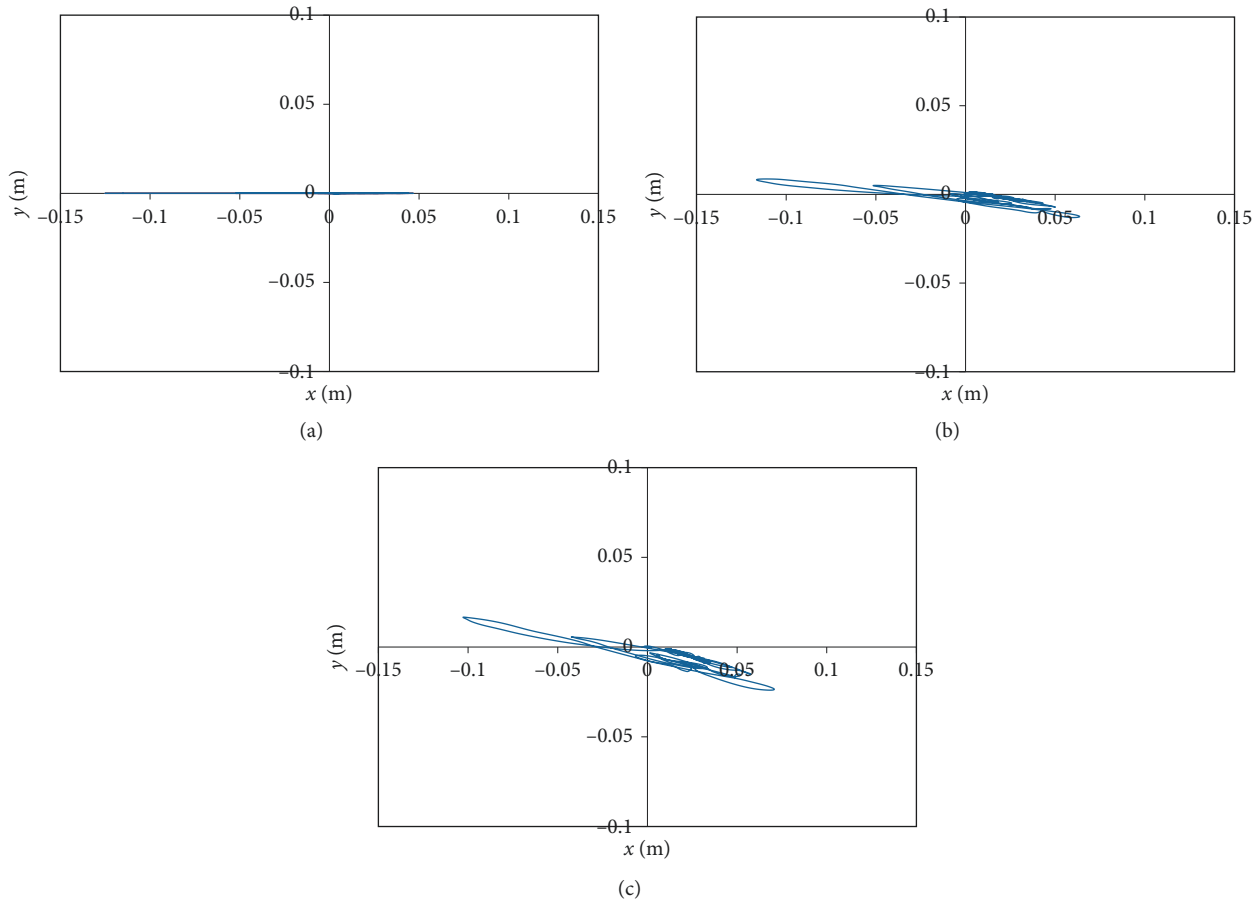

Figure 13: Four-column frame: displacements in the plane xy due to an acceleration input along x for (a) C0, (b) C3 with μ_a, and (c) C3 with μ_b.

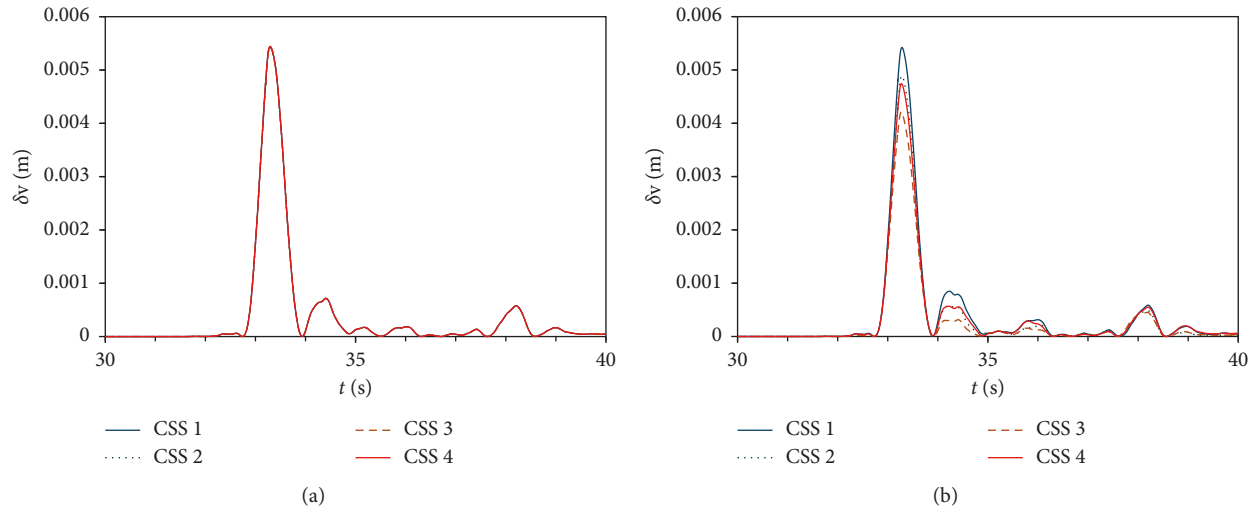

Figure 14: Continued.

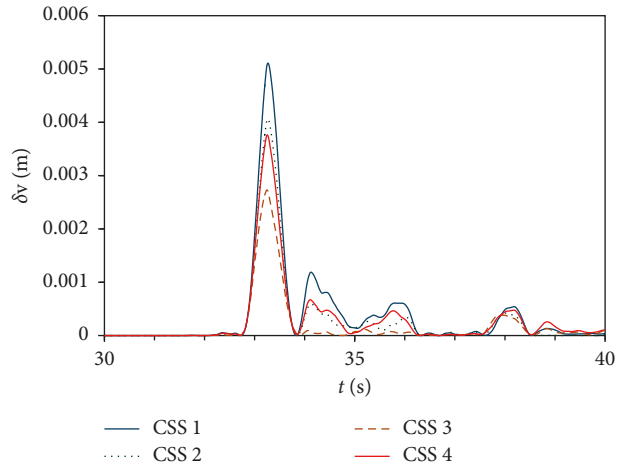

(c)

Figure 14: Four-column frame: vertical displacements with 3D input for (a) C0, (b) C3 with μ_a, and (c) C3 with μ_b.

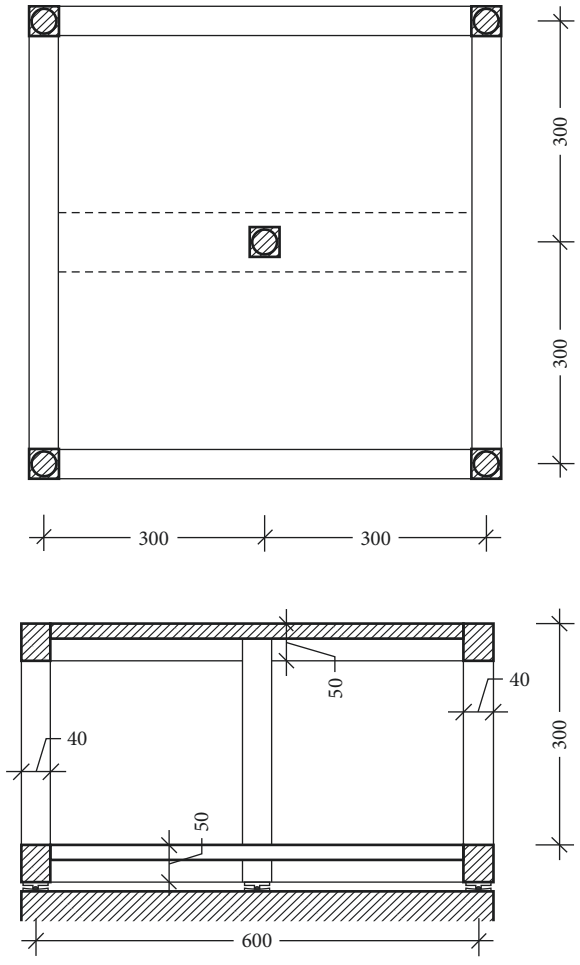

Figure 15: Five columns frame (dimensions in cm).

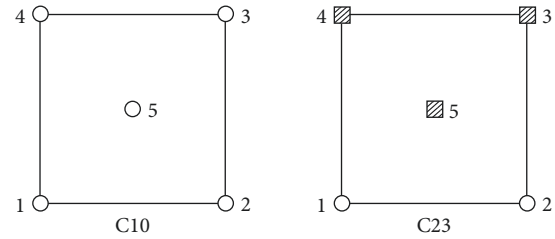

Figure 16: Five columns frame: different deployments of the sliding devices: circle = normal friction coefficient and square = increased friction coefficient.

Table 3: Five columns frame: characteristics of the four perimetral isolators.

Friction coefficient	μ	$1.5\,\mu$	$2.5\,\mu$
Secant stiffness K_e(kN/m)	379.2	238.1	307.6
Elastic shear stiffness k (kN/m)	11438.2	7181.2	9275.7
Equivalent period T_{is} (s)	3.26	3.01	2.65

vibration but also with an important rotational component. This is particularly apparent in the case C23 (Figure 16).

The nonlinear analysis showed that in the presence of acceleration only along the x axis, model C10 showed displacements along x direction only, while all the other models presented also displacement along the y axis. These were higher in the model C23 in the case μ_b (Figure 17).

The maximum variation of the vertical load is about 60%; therefore, no uplift occurred, and the displacement vertical component was consistent with Equation (9). As shown in Figure 18, the vertical displacements were always the same in C10, while in model C23, it was verified that the maximum values were reached at the same time, and in any case, the contact points of the five sliders were on a plane.

7. The Influence of the Static Friction

The static friction is usually much higher than the dynamic friction. If μ_0 is very high, then sliding could not occur, the system behaves as rigid, and there is no decoupling of

Table 4: Five columns frame: characteristics of central isolator.

Friction coefficient	μ	$1.5\,\mu$	$2.5\,\mu$
Secant stiffness K_e(kN/m)	713.7	835.6	1079.3
Elastic shear stiffness k (kN/m)	21526.1	25201.3	32551.6
Equivalent period T_{is} (s)	3.26	3.01	2.65

Table 5: Five columns frame: periods and participant masses (translation X, translation Y, and rotation Z in the vibration modes).

Mode no.	T (s)	Participant mass X	Participant mass Y	Participant mass RZ	Sum X	Sum Y	Sum RZ
1	3.259	0.001	0.999	0.335	0.001	0.999	0.335
2	3.259	0.999	0.001	0.390	1	1	0.725
3	2.750	0.000	0.000	0.275	1	1	1

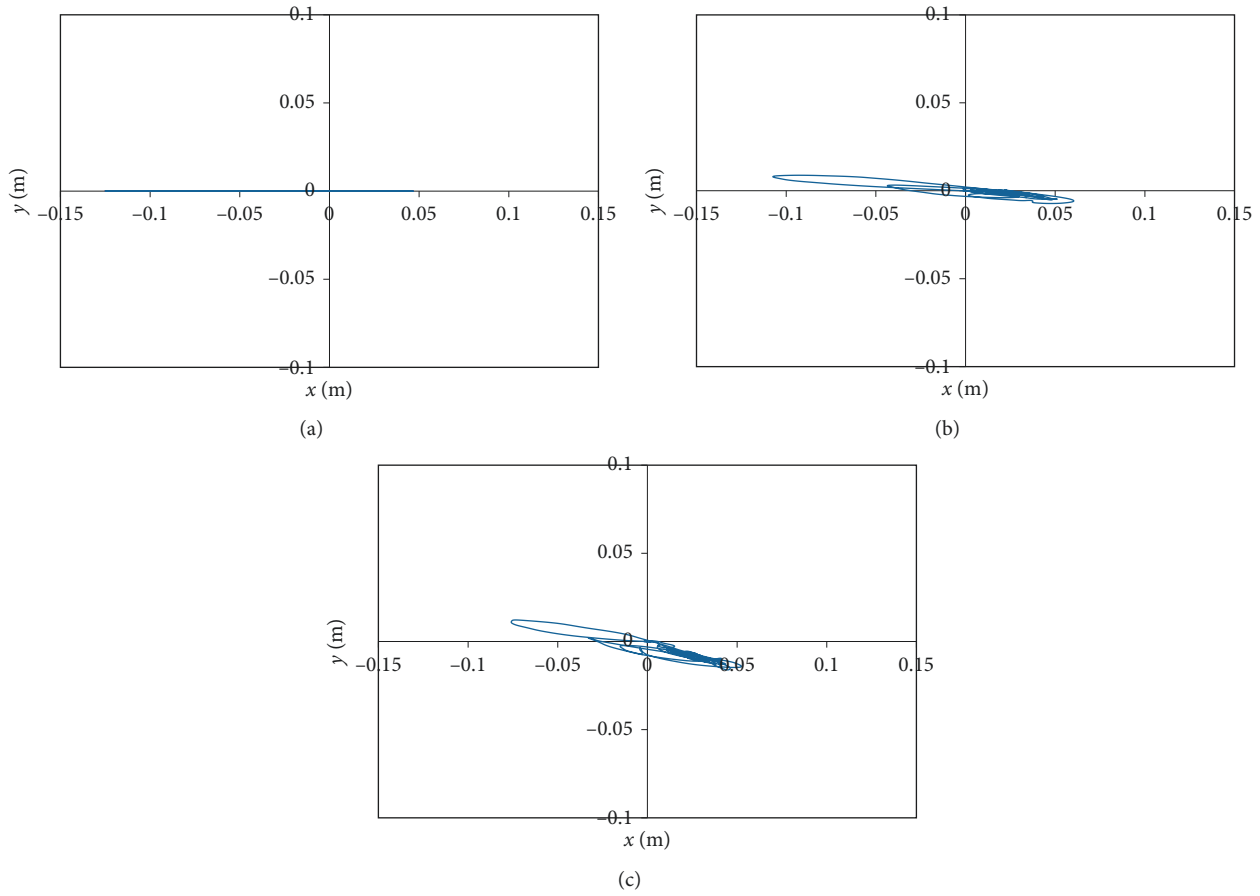

Figure 17: Five columns frame: displacements in the plane xy due to an acceleration input along x for (a) C10, (b) C23 with μ_a, and (c) C23 with μ_b.

motion between the superstructure and the soil. Furthermore, during the sliding, the stick-slip phenomenon could occur. In the following, the recordings obtained on a seismically CSS-isolated building (Figure 19) at L'Aquila, Italy, during the event of 30th October, 2016 (Mw = 6.5), are analysed and discussed.

The longitudinal components of the acceleration at the three levels are plotted in Figure 20. The amplification from the basement to the top is apparent.

The absence of the decoupling of motion is confirmed by the Fourier spectra (Figure 21), which present amplifications at frequency much higher than the design frequency of the isolated structure (equal to 0.25 Hz). In Figure 22, the time histories of the relative displacement along the longitudinal direction are plotted, between the first floor and the foundation, and between the top and the first floor, respectively. It is apparent that the isolation system is non put in action properly, due to a very high static friction.

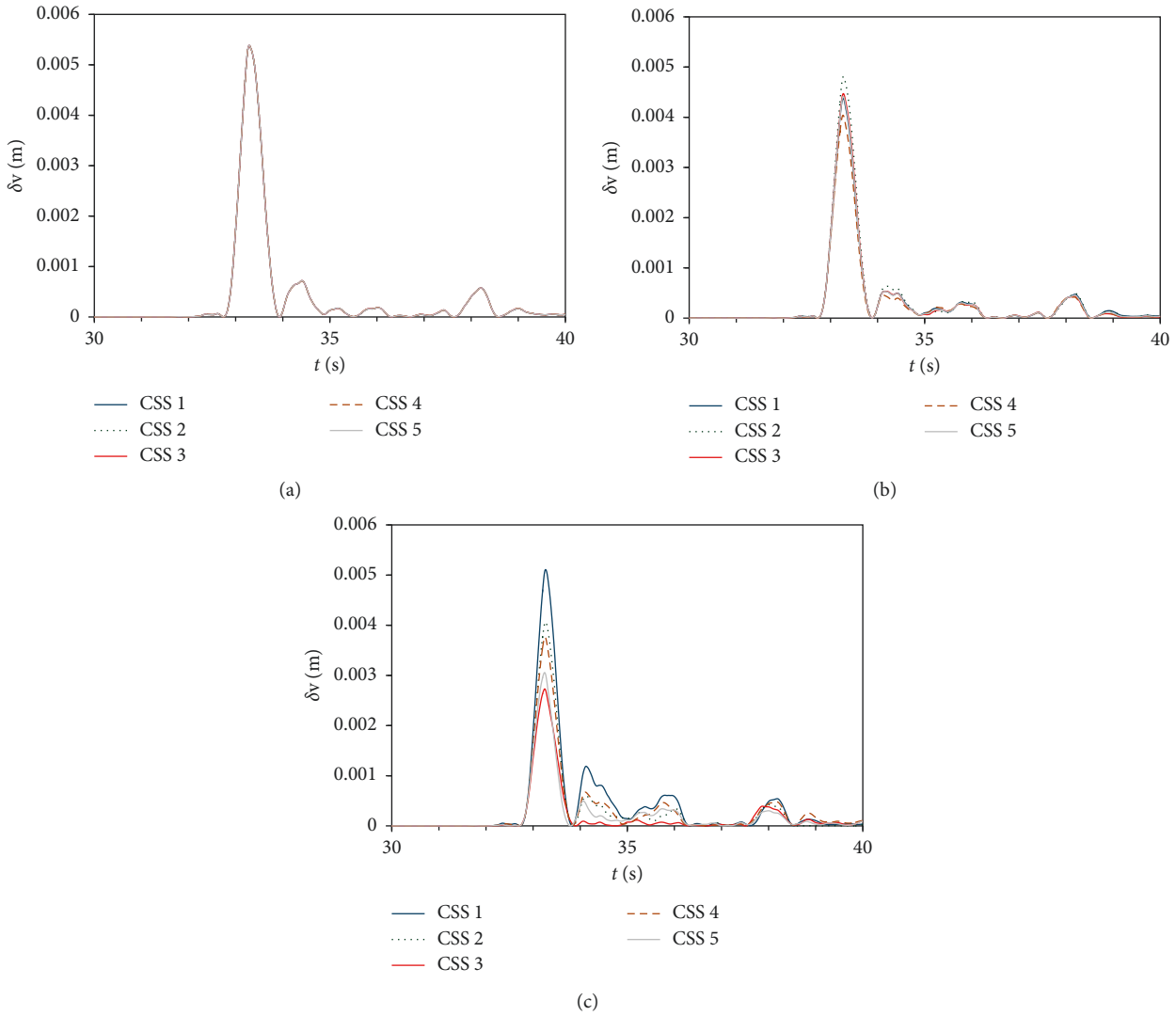

Figure 18: Five columns frame: vertical displacements with 3D input for (a) C10, (b) C23 with μ_a, and (c) C23 with μ_b.

Figure 19: The building at L'Aquila, seismically isolated by means of CSSs, deployed at the top of the circular columns, which raise up from the basement.

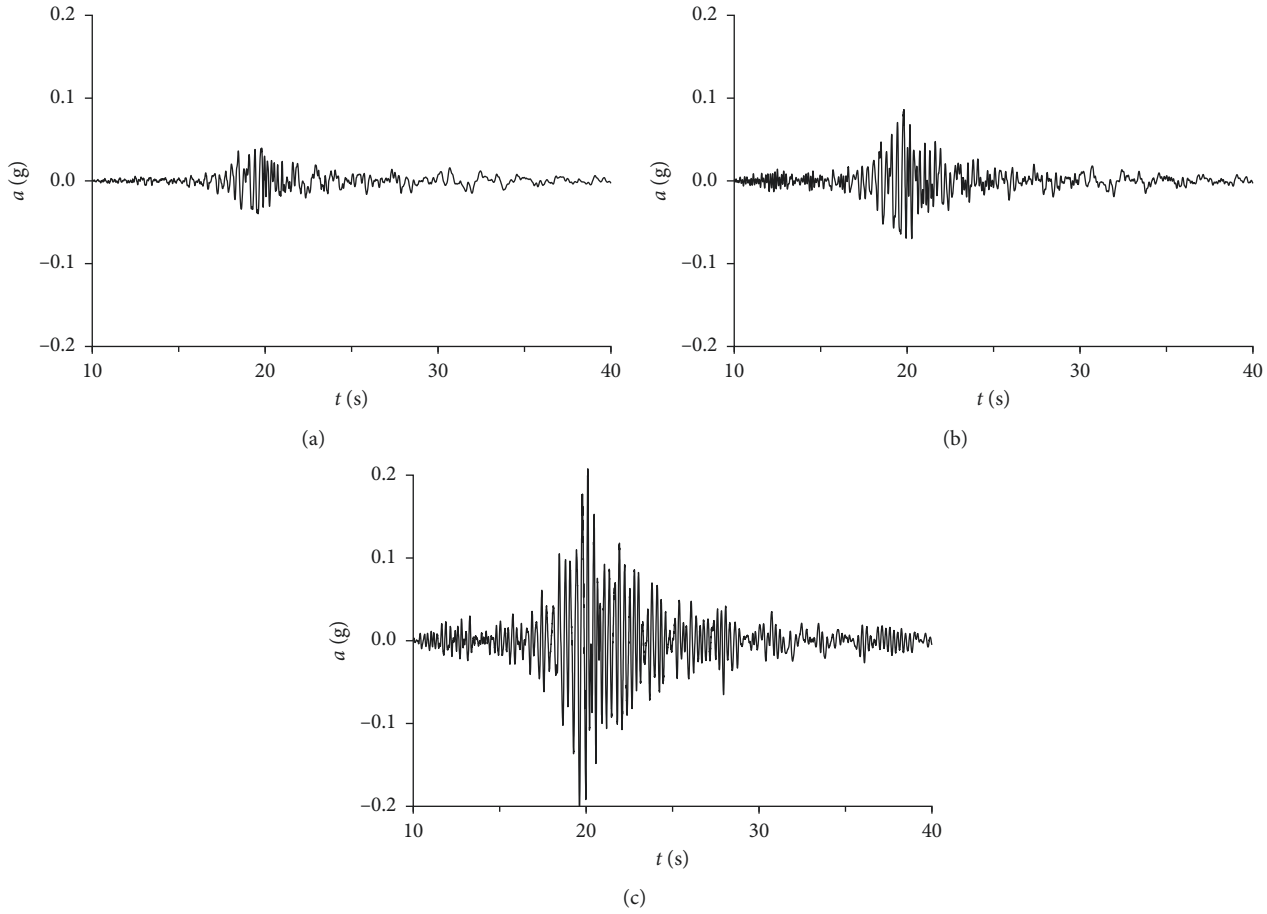

Figure 20: Accelerometric recordings obtained during the October 30, 2016, earthquake ($M = 6.5$) in the longitudinal direction (a) at the basement, (b) at the first floor just above the isolation system, and (c) at the top of the building, respectively.

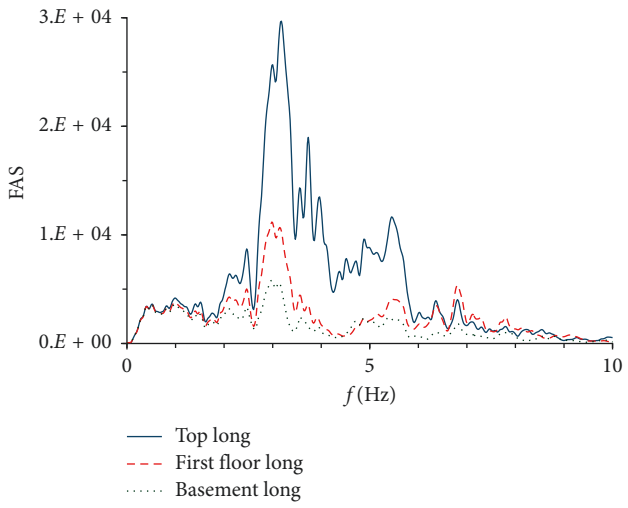

Figure 21: Fourier spectra of the time histories in Figure 20, obtained in the longitudinal direction at the basement, at the first floor just above the isolation system, and at the top of the building, respectively.

8. Conclusions

Curved surface sliders present interesting characteristics that make them very promising for a large application of base isolation in civil structures. Anyway, some features are to be studied in detail. Some of these have been analysed in this paper:

(i) The dynamic behavior of a curved surface slider is governed by three friction coefficients, relative to the onset of motion, to the dynamic phase, and to the inversion of the velocity sign.

(ii) The variability of the dynamic friction μ with the vertical load acting on it. These are different from one column to another and are also influenced by the overturning moment due to the horizontal seismic action. The effects of this occurrence has been analysed with reference to two simple framed structures, and the possibility of rotations of the superstructure has been pointed out. The rotations determine the loss of contact in some devices and also different displacements in the devices.

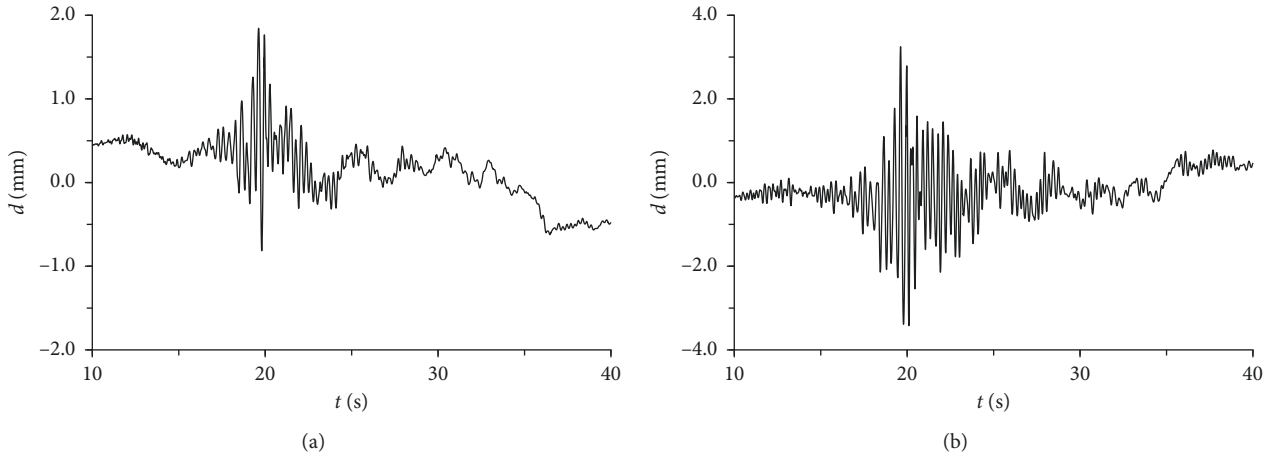

Figure 22: Relative displacement (a) between the first floor and the basement and (b) between the top and the first floor in the longitudinal direction.

(iii) The recentering of the isolation system, related to curved surface that allows the device to return to its initial position when the external horizontal action finishes, could not be guaranteed when velocity is very low; in detail, if the slider reaches the configuration with $d \leq \mu R$ with velocity equal to zero, the device will not return to its initial configuration.

(iv) The static friction should not be very high. Actually, the isolation system should have an adequate stiffness against low horizontal actions, such as wind, traffic, or low-energy earthquakes. This can be obtained by means of a suitable static friction, but this should not be so high in order to guarantee that the devices are put in action under certain seismic loadings. The importance of this aspect has been emphasized showing the experimental seismic response of an isolation system under a low-energy earthquake at the site of the building.

It appears obvious that the design of isolation systems with curved surface sliders should be done using nonlinear modelling. These should account for the static friction and the variability of friction especially with the vertical load, which makes the friction force different from one device to another.

Data Availability

The data used to support the findings of this study are available from the corresponding author upon request.

Conflicts of Interest

The authors declare that there are no conflicts of interest regarding the publication of this paper.

Acknowledgments

The monitoring of the mentioned building in L'Aquila is part of the Seismic Observatory of Structures project, organized and managed by the Italian Department of the Civil Protection (DPC Osservatorio Sismico delle Strutture–OSS Download Service, http://www.mot1.it/ossdownload).

References

[1] B. Carpani, "Base isolation from a historical perspective," in *Proceedings of 16th World Conference on Earthquake Engineering (16WCEE, IAEE & ACHISINA)*, Santiago, Chile, January 2017.

[2] M. Constantinou and A. Mokha, "Teflon bearings in base isolation. II: modeling," *Journal of Structural Engineering*, vol. 116, no. 2, pp. 455–474, 1990.

[3] G Lomiento, N Bonessio, and G Benzoni, "Friction model for sliding bearings under seismic excitation," *Journal of Earthquake Engineering*, vol. 17, no. 8, pp. 1162–1191, 2013.

[4] F. Naeim and J. M. Kelly, *Design of Seismic Isolated Structures: From Theory to Practice*, John Wiley & Sons, Hoboken, NJ, USA, 1999.

[5] P. Clemente and A. Martelli, "Anti-seismic systems: worldwide application and conditions for their correct use," in *Proceedings of 16th World Conference on Earthquake Engineering (16WCEE, Keynote lecture, IAEE & ACHISINA)*, Santiago, Chile, January 2017.

[6] P. Clemente and A. Martelli, "Seismically isolated buildings in Italy: state-of-the-art review and applications," *Soil Dynamics and Earthquake Engineering*, 2018, In press.

[7] P. Clemente, "Seismic isolation: past, present and the importance of SHM for the future," *Journal of Civil Structural Health Monitoring*, vol. 7, no. 2, pp. 217–231, 2017.

[8] A. De Stefano, P. Clemente, S. Invernizzi et al., "Innovative technique for the base isolation of existing buildings," in *Proceedings of 5th International Conference on Computational Methods in Structural Dynamics and Earthquake Engineering COMPDYN 2015*, Crete Island, Athens, Greece, May 2015.

[9] P. Clemente, G. Bongiovanni, G. Buffarini, and F. Saitta, "Experimental analysis of base isolated buildings under low magnitude vibrations," *International Journal of Earthquake and Impact Engineering*, vol. 1, no. 1-2, pp. 199–223, 2016.

[10] P. Clemente, G. Bongiovanni, and G. Benzoni, "Monitoring of seismic isolated buildings: state of the art and results under high and low energy inputs," in *Proceedings of New Zealand*

Society for Earthquake Annual Conference and 15th World Conference on Seismic Isolation, Energy Dissipation and Active Vibration Control of Structures (NZSEE2017 and 15WCSI), Wellington, New Zealand, April 2017.

[11] P. Clemente and G. Buffarini, "Base isolation: design and optimization criteria," *Seismic Isolation and Protective Systems*, vol. 1, no. 1, pp. 17–40, 2010.

[12] P. Clemente, F. Bontempi, and A. Boccamazzo, "Seismic isolation in masonry buildings: technological and economic issues," in *Proceedings of 5th International Conference on Brick and Block Masonry: Trends, Innovation and Challenges (IB2MAC)*, pp. 2207–2215, Taylor & Francis Group, Padua, London, UK, June 2016.

[13] K. L. Ryan and K. Chopra, "Estimating the seismic displacement of friction pendulum isolators based on nonlinear response history analysis," *Earthquake Engineering and Structural Dynamic*, vol. 33, no. 3, pp. 359–373, 2004.

[14] P. Clemente, F. Saitta, C. Grossi et al., "On the behaviour of buildings with curved surface sliders: consideration and preliminary analyses," in *Proceedings of 14th World Conference on Seismic Isolation, Energy Dissipation and Active Vibration Control of Structures*, University of California, San Diego, CA USA, September 2015.

[15] M. C. Constantinou, A. M. Reinhorn, P. Tsopelas et al., "Techniques in the nonlinear dynamic analysis of seismic isolated structures," *Structural Dynamic System Computational Techniques and Optimization Seismic Techniques*, vol. 12, pp. 1–24, 1999.

[16] S. Nagarajaiah, A. Reinhorn, and M. C. Constantinou, "Nonlinear dynamic analysis of 3-D-base-isolated structures," *Journal of Structural Engineering*, vol. 117, no. 7, pp. 2035–2054, 1991.

[17] Y. J. Park, Y. K. Wen, and A. H.-S. Ang, "Random vibration of hysteretic system under bi-directional ground motions," *Earthquake Engineering and Structural Dynamic*, vol. 14, no. 4, pp. 543–557, 1986.

[18] Computers and Structures Inc., *CSI Analysis Reference Manual for SAP2000, ETABS*, Computers & Structures Inc., Berkeley, CA, USA, 2009.